Received: 27 June 2023 | Revised: 8 August 2023 | Accepted: 20 August 2023

DOI: 10.1002/pen.26484

RESEARCH ARTICLE

POLYMER ENGINEERING AND SCIENCE WILEY

Tailoring 3D printed cellulose acetate properties produced via direct ink writing: Densification through over-extrusion and evaporation rate control

E. A. Slejko | **N. Sesto Gorella** | **R. Gasparini** | **N. Scuor** | **S. Seriani**

DIA—Department of Engineering and Architecture, University of Trieste, Trieste, Italy

Correspondence
E. A. Slejko, DIA—Department of Engineering and Architecture, University of Trieste, Via Alfonso Valerio 6/1, 34127 Trieste, Italy.
Email: easlejko@units.it

Funding information
European Space Agency, Grant/Award Number: AO/2-1749/20/NL/GLC

Abstract

In this study, we conducted a comprehensive experimental campaign aimed at controlling the final properties of 3D printed cellulose acetate. We equipped a commercial printer with a peristaltic pump to be able to print in a continuous fashion by means of the Direct Ink Writing technique. We investigated the effect of ink concentration and printing parameters on the density, mechanical and functional properties of printed objects. Furthermore, water absorption tests demonstrated the hygroscopic behavior of cellulose acetate, with higher water content in samples with lower densities. The diffusion of water within the polymer network followed Fickian diffusion, with the diffusion coefficient influenced by the density of samples. Overall, this study highlights the importance of printing conditions in achieving desired properties in 3D printed cellulose acetate. The ability to fine-tune the mechanical properties and water absorbance of 3D printed cellulose acetate makes it promising for applications in plant science and bioengineering.

Highlights

- Cellulose acetate has been 3D printed via Direct Ink Writing.
- The shear-thinning behavior allows for shape retention during printing.
- Density of printed samples is strongly controlled by printing parameters.
- Density of printed parts influences mechanical properties and water absorption.

KEYWORDS
additive manufacturing, peristaltic pump, polymers, water absorption

1 | INTRODUCTION

Cellulose acetate (CA) is a biodegradable and biocompatible synthetic polymer that is derived from cellulose, a natural polysaccharide found in plants. CA is produced by acetylating cellulose with acetic anhydride, resulting in a polymer with varying degrees of substitution (DS) of acetyl groups.[1–3] The DS of CA affects its physical and chemical properties, including its solubility, thermal stability, and mechanical properties. Its biodegradability and biocompatibility make it attractive for use in biomedical (drug delivery, tissue engineering, and wound healing) and commodity applications (packaging), whereas its solubility and thermal stability allow for its use in various solution-based processing methods, including 3D printing.[4–6] To obtain CA from plants, the common processes involve several chemical and physical steps. Cellulose is extracted from plant materials, such as wood

pulp or cotton fibers. This is usually done through a process of pulping, which involves breaking down the plant material in a chemical solution to separate the cellulose fibers.[7] The extracted cellulose is then chemically modified through a process called acetylation, where acetic anhydride and acetic acid are used to introduce acetyl groups onto the cellulose chains. This process creates CA, which is a thermoplastic material that can be molded into various shapes. The CA is then purified to remove any impurities and to adjust its properties, such as its molecular weight and degree of substitution. The purified CA can then be processed into various products, such as film, fibers, and plastics.[1] This can be done through processes such as extrusion, injection molding, or casting. Besides its terrestrial use, potential applications of CA are related to space system manufacturing and development of functional structures; in this case, CA may be derived from the processing and operations of carbon rich resources. In the last years, interest for advanced manufacturing technologies applied to space systems has increased, with several challenges to be addressed yet.[8–10] Cellulose derivatives can be used, for example, as structural material for the realization of light but resistant constructions, or as artificial graft to improve plant growth in harsh environments and sustain life in space. Grafting has been already proved as an efficient strategy to increase crop production by an improved nutrient intake and water usage, at the same time reducing the damage induced by soil-borne pathogens.[11–15] Thanks to its large water absorption ability, 3D printed CA structures can be used as replacements or supports to plant roots, allowing a more efficacious absorption of nutrients and, consequently, a more sustainable plant growth.

CA can be 3D printed by means of Direct ink writing (DIW), which is a 3D printing technique that uses a nozzle to extrude a liquid or semi-solid material (called ink) in a controlled manner to create 3D structures.[16,17] In DIW, the ink is usually a complex mixture of a polymer and a solvent, which allows it to flow through the nozzle and solidify after deposition.[18] The ink can also contain other additives such as nanoparticles or fibers to enhance the properties of the printed structure.[7,19] The ink solidifies rapidly after deposition, usually through solvent evaporation or crosslinking. The solvent used depends on the specific grade of CA, but common solvents include acetone, chloroform, and methylene chloride. The concentration of CA and the choice of solvent can affect the properties of the ink, such as its viscosity and solidification behavior: for example, Liu et al. investigated the properties of a mixture of CA, acetone, and water; while Huang and Dean found better printability when adding glycerol.[4,20] The ink is loaded into a syringe or nozzle and extruded onto a substrate in a controlled manner to create the desired 3D structure. After printing, the CA structure can be post-processed to improve its mechanical properties. For example, the structure can be annealed or cross-linked to increase its strength and stiffness.[21] DIW of CA has been used to fabricate a range of structures, including microfluidic channels, scaffolds for tissue engineering, and functional devices such as biosensors and actuators.[4,22,23] The versatility and biocompatibility of CA make it an attractive material for 3D printing applications in biomedicine and beyond.

3D printing CA can be challenging due to some limitations, mainly related to its melting temperature, shear thinning behavior, and solubility.[4,21,24] CA has a high melting temperature, typically around 230°C–260°C, which can make it difficult to 3D print using conventional extrusion-based 3D printers. Furthermore, CA is not very soluble in most common solvents, which can make it challenging to prepare printable ink or filament for 3D printing. Preparing a suitable ink or filament may require additional processing steps, such as dissolving the CA in a solvent and then evaporating the solvent to leave behind a printable material.[22]

One of the most common solvents for CA is acetone: the interactions between acetone and CA in solution play an important role in various solution-based processing methods, including 3D printing. Acetone is a highly polar solvent that can dissolve CA due to its ability to hydrogen bond with the acetyl groups on the polymer chains. The hydrogen bonding between acetone and CA is driven by the dipole–dipole interactions between the polar acetone molecules and the acetyl groups on the polymer chains. This interaction leads to the formation of a complex network of intermolecular hydrogen bonds between the acetone molecules and the acetyl groups on the CA chains. The interactions between acetone and CA in solution can be influenced by several factors, including the DS and the molecular weight of the polymer, the temperature of the solution, and the concentration of the solvent. For example, as the DS of CA increases, the number of available acetyl groups for hydrogen bonding with acetone also increases, leading to a stronger interaction between the two molecules. Similarly, as the molecular weight of the polymer increases, the size of the polymer chains also increases, leading to a greater surface area for interaction with acetone.[25] The concentration of the solvent can also affect the interactions between acetone and CA. At low concentrations of acetone, the number of available solvent molecules for interaction with the polymer chains is limited, leading to a weaker interaction between the two molecules. These interactions play an important role in various solution-based processing methods, including 3D printing, where the

solubility of CA in acetone is critical for the preparation of printable inks.

The state-of-the-art in DIW of CA make use of syringe pumping systems.[20,26,27] This has the major drawback of a discontinuous fabrication, and it is not applicable for large parts without considering complex operations of syringe refilling, which may cause a poor quality of the final printed part due to the interruption of the process. In this contribution, we aim at demonstrating the applicability of a continuous production of CA 3D printed parts by means of a peristaltic pump. Furthermore, common solutions of CA in acetone for DIW do not exceed a percentage of 35%.[20,28] Several studies have been conducted on the properties of the ink, but few took into consideration the effect of printing parameters on the final quality of printed parts. As the maximum concentration of CA inside the printing ink currently represents a technological limit, as small pumping systems are not able to operate solutions beyond a certain viscosity. For example, Pattinson and Hart reported that typical extrusion pressure is in the order of 1 MPa.[26] Therefore, it is worth considering other strategies to tailor the final properties of 3D printed parts. In this contribution, we aim at investigating how the most common printing conditions affect the density and mechanical properties of CA samples printed by means of Direct Ink Writing.

2 | EXPERIMENTAL SECTION

2.1 | Materials

CA powder (M_n = 29,000 g/mol, degree of acetylation = 2.5, acetyl content = 40%) and acetone (>99.8% purity) were purchased from Fluka and Sigma Aldrich, respectively. Acetone was selected because it is a cheap solvent with a high vapor pressure that evaporates quickly and may be recycled if condensation systems are used.

To prepare a printable ink, CA powder was dissolved in acetone and stirred overnight in a sealed backer to obtain a viscous and homogeneous solution. Four different concentrations of CA in acetone have been investigated: 20% w/w, 25% w/w, 27% w/w, and 30% w/w. For the investigation of the printing parameters, a batch solution of CA in acetone at 25% w/w has been prepared.

2.2 | Pumping system

The main problem related to the Direct Ink Writing (DIW) printing technique is identified in the material extrusion process. Usually, the printing material is stored inside contused volumes such as syringes that are then pressed by a linear actuator. This solution allows only small volumes to be printed or makes it necessary to interrupt the process for the reservoir refill.[29] A versatile extruding system, independent form the printing volume, is obtainable by replacing the linear actuator with a volumetric pump, such as a peristaltic pump. The design of the pump used in our experimental campaign is reported in Figure 1A. A peristaltic pump offers multiple advantages, for example it can displace aseptically various fluids and it does not limit the printing volumes to the contents of a syringe while achieving a precise dosage control.[30]

The volumetric flow rate of a peristaltic pump is identified by Equation (1).

$$Q_{\text{nom}} = \pi \cdot r_i^2 \cdot \omega \cdot (r_h - r_o) \tag{1}$$

r_i and r_o are the inner and outer radius of the silicone tube respectively, ω the angular velocity of the pump and r_h is the peristaltic pump housing radius.[31] However, the presence of the roller reduces the displaced volume V_{rot} from its nominal value V_{nom} as indicated in Equation (2).

$$V_{\text{rot}} = V_{\text{nom}} - V_r * N_r \tag{2}$$

where V_r is the volume of the silicone tube occupied by a single roller and N_r is the number of rollers of the peristaltic pump. Therefore, the average volumetric flow rate Q_a of the peristaltic pump is obtained as

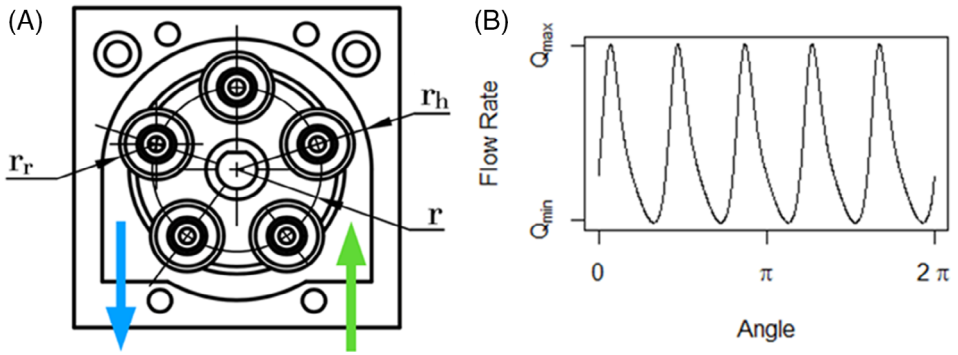

FIGURE 1 (A) Design of the 5-rollers peristaltic pump use in this work and (B) qualitative representation of the oscillatory feed rate for a complete rotation of the pump head. The difference between $Q_{\max}$ and $Q_{\min}$ represents the amplitude of the volumetric flow rate.

$$Q_a = \frac{V_{\text{rot}} * \omega}{2\pi} \tag{3}$$

The major disadvantage of this pumping systems is represented by the pulsing at their output pressure (Figure 1B). Pulsation is caused by the material redistribution caused by the engaging and disengaging of the rollers on the silicon tube. In DIW printing, the oscillatory pressure produces an alternate lack or excess of the printed material, lowering the dimensional accuracy of the print. The pulsating component Q_p of the volumetric flow is determined by Equation (4).

$$Q_p = \frac{dV_r}{dt} \tag{4}$$

There will be multiple back-flow pulses equal to the number of rollers for each complete revolution of the rotor, and the frequency is provided by the number of rollers multiplied by the rotor angular velocity, given by

$$F(\text{Hz}) = \frac{N_r * \omega}{60} \tag{5}$$

Although we did not record any major deviation from the nominal dimensions of our samples, the pulsating flow rate is a limitation to keep in mind when printing components (especially small ones) requiring extreme dimensional accuracy. For a more detailed analysis of the performance of peristaltic pumps, we address the reader to some recent articles.[29–32]

2.3 | Printer modification and experimental campaigns

A Creality Ender 3 was chosen as the basis for building a Direct Ink Writing-type 3D printer. The main characteristics of the printer are shown in Table 1. To transform a Fused Deposition Modeling (FDM) printer to a DIW printer, modifications to the original printer were needed. The DIW technique is ideal for printing materials in liquid form such as solutions of CA in acetone (Figure 2A), a working condition that does not required the printed material to be heated. Therefore, the first step involved removal of the hot end and the extruder. The extruder has been replaced by a 5-roller peristaltic pump for handling CA inside a silicone tube of diameter (3 mm) while the hot end has been replaced by an extrusion nozzle of diameter 0.3 mm. The CA ink is stored inside a sealed reservoir during the entire printing process. To ensure greater adhesion to the printing plate, the original polymer sheet covering the printing plate was replaced with a layer of Kapton® tape (Figure 2B).

TABLE 1 Creality Ender 3 printer characteristics, as specified on the manufacturer's website.

Specifications	Value
Build volume [mm × mm × mm]	220 × 220 × 250
Resolution [μm]	100–300
Filament diameter [mm]	1.75
Nozzle diameter [mm]	0.4
Hot-end setup	Bowden
Maximum print speed [mm/s]	180
Maximum extruder temperature [°C]	250
Maximum build plate temperature [°C]	100

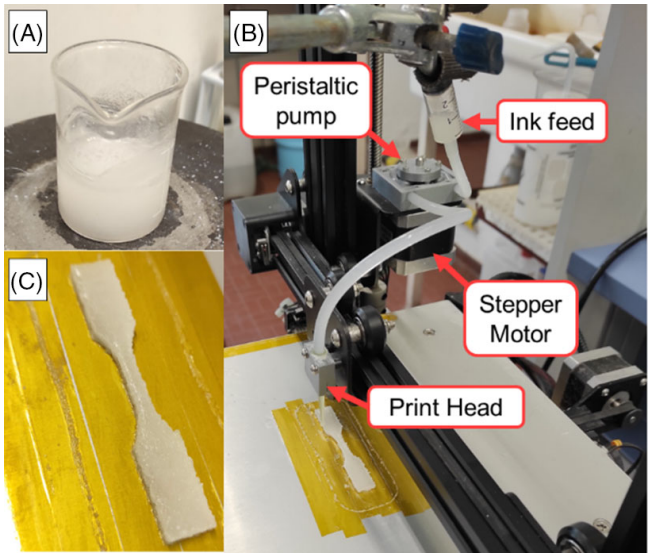

FIGURE 2 (A) Starting CA ink for the printing experiment. The ink is always kept in a sealed container to avoid evaporation of the solvent. (B) Overview of the printing equipment. (C) Standard 3D printed sample.

2.3.1 | Ink concentration campaign

One experimental campaign was conducted to qualitatively investigate the influence of the CA ink concentration and its effect on the printed specimens' quality (i.e. mechanical and thermal properties, shape and structural stability). The campaign was conducted using inks with CA concentrations varying between 20% w/w and 30% w/w; the other printing parameters are indicated in Table 2. Specimens were printed according to the dimensions of the Type V specimen described in the ASTM

TABLE 2 Printing parameters for the ink concentration campaign.

Parameter	Value
Line width (mm)	0.4
Layer height (mm)	0.2
Print speed (mm/s)	20
Infill density (%)	100
Raster orientation	+45°/−45°
Bed temperature (°C)	45

D638-03 standard; an example of a printed sample is reported in Figure 2C.

2.3.2 | Feed rate and evaporation control campaign

A second campaign has been performed to investigate the effect of the feed and evaporation rates. E-step values and plate temperature have been varied in the range of 50–150 mm^{-1} and 30–50 °C, respectively. The other parameters are indicated in Table 3. Ink with a CA concentration of 25% w/w has been used in all experiments of this campaign.

To estimate the feed rate during printing, we used the formulation in Equation (6). The feed rate Q is calculated based on the nozzle radius r and the feed velocity v_f. This last quantity is linearly dependent on the E-step value, since increasing the rotation of the stepper motor would cause more material to be extruded.

$$Q = \pi r^2 v_f \tag{6}$$

The value of the feed rate is fundamental when considering the rheological behavior of the ink, as larger feed rates imply greater shear stresses. The feed rate of the printer has been calibrated by extruding single strands of ink based on a defined geometry, measuring the mass of the printed material immediately after printing as a function of the selected E-step values. Results of the calibration procedure are reported in Table 4.

2.4 | Characterization

2.4.1 | Density

To reach complete evaporation of acetone, printed samples have been left conditioning in a dry box for 3 days. Their density has been estimated by dividing their weight for the expected volume, as provided by CAD design. Even if this represents a limitation since size deviations are often introduced while printing via DIW, the use of the design volume for the evaluation of relative density does not affect the observed trends. Relative density has been calculated by dividing the measured density of the sample by the reference density of bulky CA (equal to 1.3 g/cm^3).[33]

TABLE 3 Printing parameters for the feed rate and evaporation control campaign.

Parameter	Value
Line width (mm)	0.3
Layer height (mm)	0.2
Print speed (mm/s)	50
Infill density (%)	100
Raster orientation	+45°/−45°

TABLE 4 Results of the feed rate calibration. The starting ink had a density of 0.71 g/cm^3 and the average printing time was 8.32 seconds.

E-step	Mass (mg)	Calculated feed rate ($mm^3\ s^{-1}$)
50	22.7	3.9 ± 0.6
60	35.0	5.9 ± 0.9
100	24.0	4.1 ± 0.6
150	45.5	7.7 ± 1.2

2.4.2 | Mechanical

Uniaxial tensile tests and flexural tests, using a Shimadzu AGS-X test system with a 10 kN load cell, were performed to measure ultimate strength, modulus, and elongation at break. Testing has been carried out in accordance with ASTM D638-03 and ASTM D790-03.

2.4.3 | Thermal

Differential Scanning Calorimetry (DSC) has been carried out using a Netzsch DSC 200 F3 Maia equipment to examine the thermal behavior of samples. In aluminum crucibles, 5 mg of material was heated at a rate of 10 °C·min^{-1} from 50 °C to 300 °C. The materials' thermal stability was assessed using a thermogravimetric analysis, or TGA. Alumina crucibles containing 5 mg of the sample were heated using a Netzsch STA 409 EP instrument from 50 °C to 600 °C at a heating rate of 10 °C·min^{-1}.

2.4.4 | Rheological

Rheological characterization was carried out by means of a TA Instrument Discovery Hybrid Rheometer HR1. The tests were conducted at 20 °C using a plate-plate geometry (25 mm in diameter with the plates being 300 μm apart). During the test, a solvent trap was installed to avoid solvent evaporation. The viscosity was measured at shear rate of 0.05–500 s^{-1}.

2.4.5 | Infrared spectroscopy

Spectra of 3D printed samples were collected using a Thermo Nicolet Nexus 470 Fourier Transform IR spectrometer equipped with an Avatar Diffuse Reflectance accessory. The spectra were obtained between 400 and 4000 cm^{-1}; the spectrometer's nominal resolution was 2 cm^{-1}.

2.4.6 | Thermomicrography

Drops of CA solution at 25% w/w have been casted on alumina substrates and placed in a heat chamber. Temperature has been varied from 30 °C to 59 °C, while the shape change of the drop has been recorded by means of a digital camera connected to the microscope.

2.4.7 | Water absorption

Before the test, samples have been conditioned in an oven at 50 °C for 24 h, stored in a desiccator and weighed immediately before immersion (m_0). The samples are then immersed in deionized water and their weight is measured after 2 and 24 h (m). Test has been conducted accordingly to ASTM D570-98. The absorbed water ratio W has been calculated by Equation (7).

$$W = \frac{m - m_0}{m_0} \tag{7}$$

3 | RESULTS AND DISCUSSION

By observing the change in viscosity with increasing shear rate, the shear-thinning behavior of the CA inks was assessed (Figure 3A). The shear thinning behavior displayed by all inks is typical of pseudo plastic fluids, which have low viscosity at high shear rates and vice versa. This is due to the motion of CA molecules, which tend to disentangle when shear is applied, reducing their flow resistance. Consequently, viscosity decreases at high shear rates.[4,20,34] This is a fundamental characteristic for printable inks: they should flow when shear stress is applied to facilitate extrusion, but at the same time they should retain their shape once the shear stress is removed to avoid the collapse of the printed object.

Chemical characterization (Figure 3B) by means of FTIR spectroscopy has been conducted on CA powder and samples printed with inks having concentrations of 25% or 27% w/w. The FTIR spectra of 3D printed CA have a distinctive peak at 1736 cm^{-1}, which is connected to C=O stretching. The peaks at 2948 cm^{-1} are attributable to the symmetric and asymmetric C–H stretching vibrations of methyl groups, while those at 1431 and 1368 cm^{-1} correspond to the symmetric and asymmetric C–H bending vibrations, respectively. In addition, the peaks at 1219 and 1031 cm^{-1}, which are associated to the C–O–C groups, are indicative of cellulose molecules. Finally, the out-of-plane bending of OH groups is thought to be responsible for the peak at 902 cm^{-1}.[26] The identical FTIR spectra of CA powder and 3D printed samples show that they have comparable chemical composition and structure. It is worth noting that the peak at 1703 cm^{-1}, attributed to the carbonyl group of acetone and clearly shown in the 25% wet spectrum, is missing from dry samples since complete acetone evaporation has been achieved before FTIR analysis.[35]

Thermal characterization of CA powder and printed samples is presented in Figure 3C,D. DSC curves indicate the typical melting process at 230°C, while TGA trends show the standard degradation temperature at 355°C for all samples, in accordance with the literature.[36,37]

Relative density and tensile test results for the ink concentration campaign are shown in Figure 4. As can be seen, the density of printed samples is measured in the range 30%–36%, even when starting with CA concentrations in solution as low as 20%. This can occur due to acetone evaporation during printing, which subsequently leads to the densification of the sample. As expected, the higher the initial solution concentration the larger the final measured density. Observed tensile resistance is in the range of 32 to 37 MPa, while deformation at rupture is measured between 10% and 13%. These values are consistent with reference samples found in the literature.[20] The reported mechanical properties do not present significant and clear trends. We believe this is caused by a synergetic effect of multiple factors: while, on one side, an increase in CA concentration would produce denser samples, on the other hand the homogeneity may not be sufficient due to limited ink flow. As a consequence, imperfections and defects are introduced in the material.

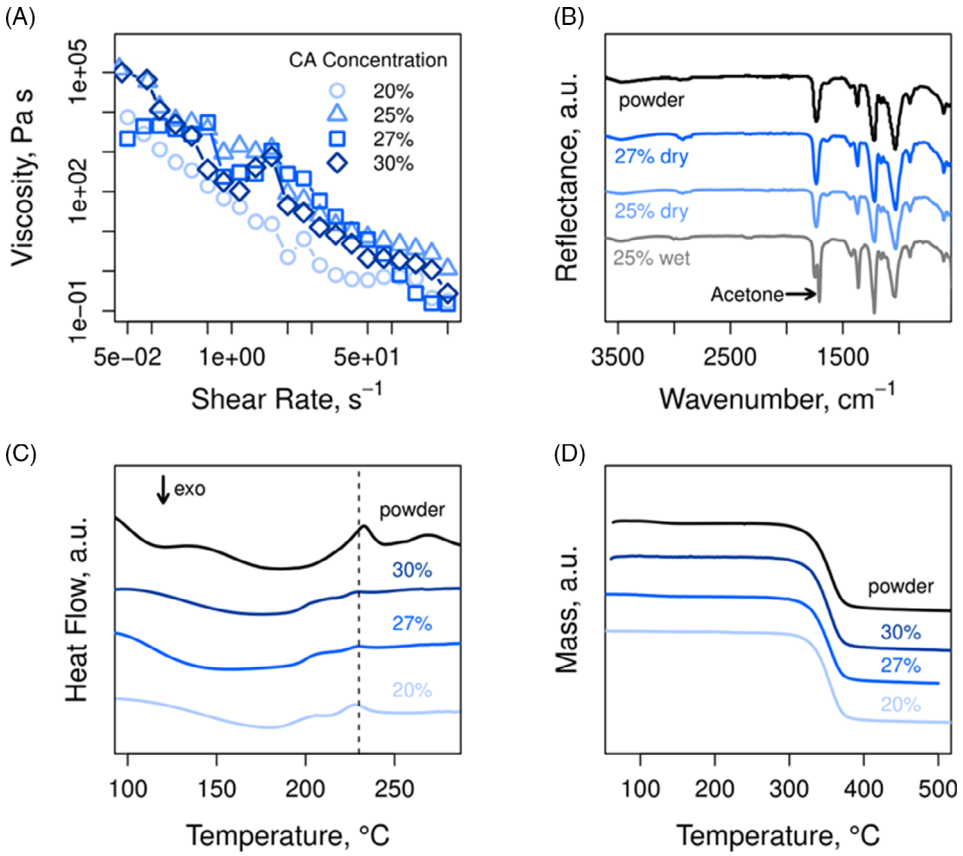

FIGURE 3 (A) Rheological characterization of the starting ink: all compositions indicate a shear-thinning behavior during the flow sweep test. (B) FTIR spectra of printed samples; the peak at 1703 cm^{-1}, associated to the presence of acetone, is indicated by the arrow on spectrum 25% wet. Thermal characterization of printed samples: (C) DSC curves and (D) thermogravimetric analysis.

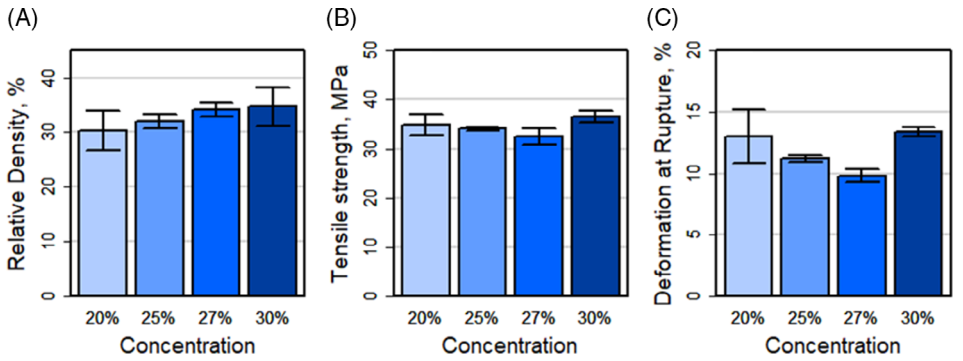

FIGURE 4 Mechanical characterization of samples printed from increasing concentration of CA in the starting ink. (A) relative density, (B) tensile strength and (C) deformation at rupture.

This could be the interpretation of the slightly lower tensile strength and deformation at rupture for the 25% and 27% CA concentrations. Nevertheless, this behavior is quite interesting, because it indicates that the common range of solution concentrations does not allow sensible tailoring of the final properties of 3D printed parts. To adjust the final properties, more concentrated solutions have to be used, but this is technologically limited unless complex and massive pumping systems are used.[26] In fact, lower CA concentrations would produce a fluid ink unable to retain its shape during printing; on the opposite end, higher concentrations would be difficult to extrude due to their viscosity. These aspects are observed in multiple literature sources, all indicating the best range of CA solutions with acetone between 20% and 35%. The observed behavior, therefore, indicates that other strategies have to be applied aiming at tailoring the printed part mechanical properties.

We used the additional solution at 25% w/w CA in acetone to investigate the effect of printing parameters on the properties of printed parts. Two main parameters have been varied in our experiments: E-step and plate temperature. The E-step value is related to the amount of extruded material per unit length; the larger this value the more ink is deposited. The plate temperature is associated with the evaporation rate of the solvent, that is, acetone. High temperatures would allow fast evaporation and, as a consequence, the densification of the printed object as the material shrinks. We therefore expect that a

higher plate temperature would allow larger E-step values, since a fast evaporation of acetone would signify the possibility to extrude a larger fraction of ink. Results of this experiment are reported in Figure 5A. The observed metric to quantify the effect of E-steps and plate temperature is the measured density of the printed object. As can be seen, for low values of plate temperature the trend is the expected ones: larger values of E-step are associated to larger densities and an increase in temperature causes an increase in the measured density irrespective of the E-step value. In the range of 35°C–40°C, this trend is inverted: increasing the temperature causes a decrease of the part density. This is associated to an excessive over extrusion, which causes the part printing to fail as portions of the extruded ink are deposited, for example, on the nozzle or are carried outside the geometry of the object due to the motion of the print head. The effect of this inefficient deposition is that printing failed and the part presented a lower density due to material waste. The observed over extrusion at high temperatures is mainly associated to the easier flow and reduced shape retention characteristics of the ink, resulting from the change in viscosity of the material. Furthermore, an enhanced evaporation rate of acetone would cause an unstable extrusion and ink deposition, making the printing process difficult to maintain over time.

The E-step value is associated to the feed rate, which represents the amount of material being extruded. If we represent the relationship between feed rate and observed density, we identify a linear trend irrespective of plate temperature (Figure 5B). This is consistent with Equation (6). An increase of the feed rate means more ink is extruded and the density of the final printed object increases as well.

The behavior observed in Figure 5A can be associated to the lower diffusion of solvent through the solid polymeric skin formed during the evaporation from the surface of the deposited strand. To substantiate this idea, we performed a series of thermal micrographs of ink drops, analyzing the variation of the cross section of the drop. Temperature has been changed from 25°C to 60°C, allowing complete evaporation of acetone.

A polymer-rich region forms on the surface of the ink drop during solvent desorption (Figure 6). The skin begins to form when the polymer concentration reaches a specified value (gelation point).[38] As a result of desorption, solvent from the liquid region penetrates the skin and passes through the porous structure. A substantial pressure gradient is required to pull the solvent through the porous network in this manner.[39] Since the pressure gradient in the skin governs the solvent flow, the liquid flux at any given moment may be calculated using Darcy's equation, which relates the flux to the pressure gradient.

$$J_z = -\frac{k}{\mu}\frac{\partial p}{\partial z} \tag{8}$$

In Equation (8), k is the permeability of the skin and μ is the viscosity of the solvent. When the polymer reaches its gelation point, the permeability is expected to decrease, resulting in a lower flux. Consequently, the internal pressure rises due to solvent evaporation at temperatures close to the boiling point of acetone. This pressure gradient induces strains inside the skin layer, which may deform in response to the tensional state. Drop skin expansion may generate openings within the polymeric

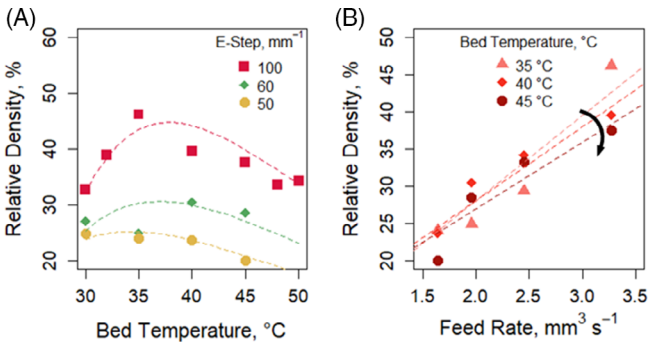

FIGURE 5 (A) Relative density of printed samples as a function of plate temperature and E-step value. (B) Influence of the feed rate and plate temperature on the relative density of printed samples.

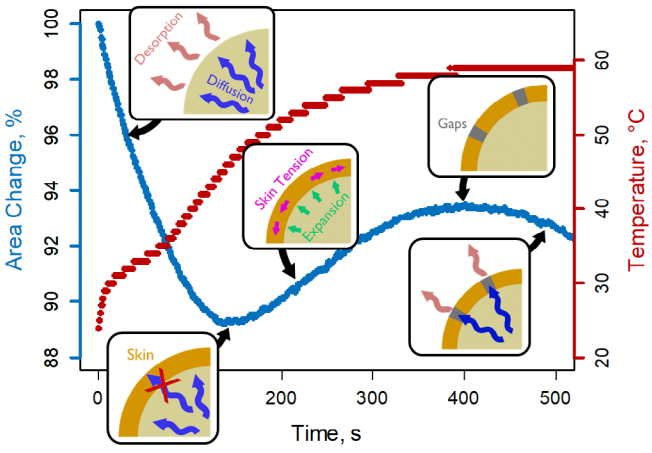

FIGURE 6 Analysis of the cross section of CA ink drops as a function of temperature: profile of the temperature ramp (red line) and measured variation of the cross section area (blue line) of the ink drop. The cross section reduction is interrupted by the formation of a skin layer (subjected to mechanical stresses due to internal pressure caused by solvent evaporation). The area reduction proceeds again when the continuous skin layer is interrupted (gaps) and acetone can flow outside the drop.

gel structure, for example due to disentanglement of polymeric coils, allowing for easier permeation through the skin. As a result, desorption proceeds further and the cross section of the droplet decreases once more. We believe the intermediate expansion stage, observed in the temperature range of 40°C–60°C, is responsible for the lower quality and dimensional instability of printed samples reported in Figure 5A. The expansion causes oozing of material and nozzle clogging during printing and, as a consequence, a failed part. The observed temperature range associated to drop expansion is in accordance with the printing plate temperatures at which failure of samples starts to occur.

Mechanical properties of sample printed at various E-step values are reported in Figure 7A–D. As can be seen, increasing the E-step determines a denser printed sample, with an analogous trend for the elastic modulus and, to some extent, to the tensile strength of the material. It is well known that there is a direct relationship between the density of a material and its modulus: the elastic modulus E can be written as the ratio between stress σ and strain ε, which are proportional to the applied external force F over the resisting area A and the relative change of length of the sample ($\Delta L/L$)

$$E = \frac{\sigma}{\varepsilon} = \frac{F}{A}\frac{L}{\Delta L} \tag{9}$$

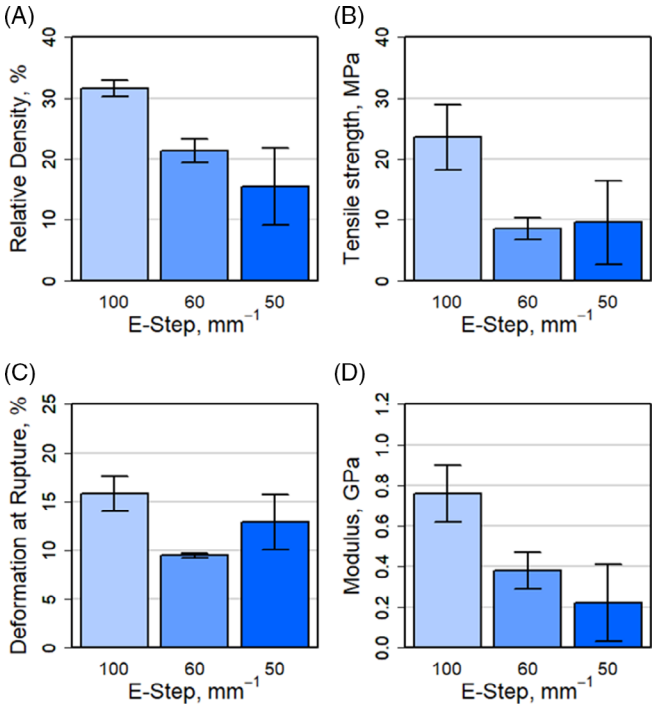

FIGURE 7 Mechanical characterization of printed samples with different E-step values: (A) relative density, (B) tensile strength, (C) deformation at rupture and d) elastic modulus.

By multiplying for L, Equation (9) reads

$$E = \frac{FL^2}{(AL)\Delta L} \tag{10}$$

The term in round brackets represents the volume V of the sample, and by substituting the definition of density ρ as the ratio between mass m and volume V, we obtain

$$E = \frac{FL^2}{m\Delta L}\rho \tag{11}$$

Equation (11) clearly indicates the theoretical relationship between modulus and density. Rearranging it, we can write

$$E = E_0\left(\frac{\rho}{\rho_0}\right) \tag{12}$$

In Equation (12), E_0 represents the modulus of the bulk material (with $\rho_0 = 1.3$ g/cm^3).[33] The term in round brackets, therefore, indicates the relative density of printed samples. The linear trend is reported in Figure 8A, where the flexural modulus is measured for various samples with different densities. The slope of the dashed line indicated in the plot is very close to the literature value of the flexural modulus for a bulky sample of CA, which is around 4 GPa.[37] The lower value of the slope and, therefore, the predicted flexural modulus for the bulk material may be associated to the unavoidable defects and voids created during 3D printing. While depositing layers of material, perfect and complete volume filling is not achievable because of the viscous flow of the ink. This effect strongly depends upon layer height and line width.[40]

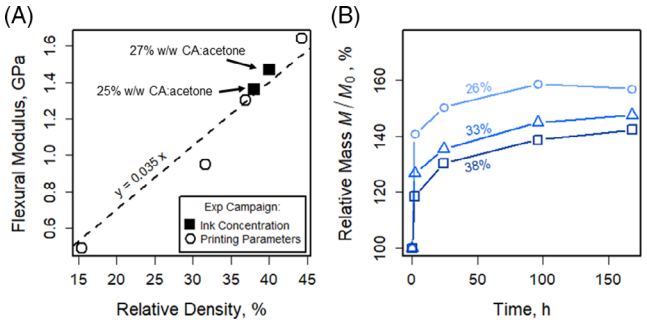

FIGURE 8 (A) Flexural modulus of samples with increasing relative densities, as obtained from the CA concentration campaign and from the feed rate and evaporation control campaign. (B) Water absorption as a function of time for sample with different relative densities.

From Figure 8A we can appreciate also the wider degree of control over the properties of 3D printed samples by varying the printing parameters, compared to the limited observed range of density (and mechanical properties) obtained when using different concentration of CA in the starting ink. This indicates that printing conditions have a strong influence on the quality and characteristics of printed materials, and therefore are a critical feature for the optimization of the object properties, as already reported in literature for, for example, polymers printed by Fused Deposition Modeling.[41–44]

To be used for the development of artificial roots, a material should possess specific characteristics related to its water absorption. Indeed, CA is a hygroscopic material that tends to absorb water and moisture. As a result, water absorption can cause swelling, shrinkage, deformation and a change of rigidity of the polymer. Experimental absorption as a function of time is reported in Figure 8B: as can be seen, three different samples with increasing densities have been tested: 26%, 33% and 38% relative density. Cellulose-based materials are well known for their hygroscopic behavior, mainly related to the presence of hydroxyl groups inside the molecular chains of cellulose. As indicated by the results, the water content increases with time, with a larger content of water inside samples with low density. Lower densities are associated to a larger free volume where water can diffuse and, therefore, a faster kinetics and a larger final content of water are expected. The diffusion of water inside polymers can be divided in three different classes, based on the relative rate of diffusion and polymer relaxation: if the diffusive transport rate is higher than polymer relaxation we talk about Fickian diffusion; otherwise we are in a Case-II condition.[45–48] When the two rates are comparable, the third class is defined as anomalous or non-Fickian diffusion. Analytical models have been introduced for studying the absorption/retention of solvent from polymers; one of the most common is the empirical power law equation derived by Crank and reported in the general simplified form in Equation (13).[45,49,50]

$$\frac{M}{M_\infty} = kt^n \tag{13}$$

where M is the mass of water absorbed at time t, M_∞ is the mass of water absorbed at equilibrium, k is a characteristic constant and n is the diffusional exponent. By fitting our experimental data with Equation (13), the values of k and n can be determined. They are reported in Table 5: as can be seen, the value of the diffusional exponent is always lower than 0.43, a critical threshold below which the mechanism of transport can be reconducted to Fickian diffusion.[51] This is consistent with the shape of the water absorption experimental data in Figure 8B, where no sigmoid trend is observed (characteristic of a Case-II transport as reported by Khoshtinat et al.[52]). The Fickian diffusion can be related to the high concentration of water into the external layer of CA samples, as a result of the wet test condition of our experiments, causing a smooth concentration profile of permeant into the thickness of the material. In fact, the anomalous diffusion has been linked to the presence of a sharp interface that separates the swollen external rubbery layers of the material from the inner dry glassy regions.[48] Mechanical stresses are associated with this configuration, resulting in an anisotropic diffusion coefficient. It is believed that our smooth and homogeneous diffusion is related to the low density of our samples, while anomalous diffusion has been reported for bulky thin membranes of CA.[52] Our interpretation is supported also by the trend in the characteristic constant k: its value is proportional to the diffusion coefficient of the system.[49,50] In our experiment, lower densities are associated to an easier diffusion of water molecules within the CA network. As a result, the diffusion coefficient is expected to be large in low density samples.

TABLE 5 Values of the characteristic constants and diffusional exponent for water absorption power law of samples with increasing relative density.

Parameter	26%	33%	38%
Characteristic constant k	0.678 ± 0.019	0.488 ± 0.022	0.374 ± 0.009
Diffusional exponent n	0.082 ± 0.010	0.133 ± 0.005	0.187 ± 0.003

The ability to fine-tune the mechanical properties (within the range of natural plants' roots) and water absorbance on 3D printed CA is an important characteristic for potential applications in plant science and bioengineering.[20,53]

4 | CONCLUSIONS

In this contribution, a detailed analysis of the properties of 3D printed CA standard samples has been presented. The extrusion-based printer has been modified to be able to work in a continuous fashion by means of a peristaltic pump. This setup is an important feature for the fabrication of large and extensive objects via Direct Ink Writing. The preservation of chemical and thermal properties, while providing a wide degree of control in terms of density and mechanical properties, indicates the effectiveness

of this fabrication configuration. The right combination of printing parameters allows a greater control on the final properties of printed objects, a strategy that relies on the proper balance between the evaporation and the feed rates. The proposed approach is especially beneficial when compared to the state-of-the-art strategies of CA 3D printing, which usually rely on increasing the concentration of CA in the starting ink but result only in limited improvements of the mechanical properties. Better results are obtained by adapting the printing parameters to the desired final characteristics of the printed object. The water absorption properties of printed CA indicate that lower densities are associated to faster kinetics and a larger final content of absorbed water. The ability to control the density and the mechanical properties of CA printed objects is critical for the development of functional structures for applications in the context of bioengineering and plant science, where the renewable and biological nature of CA is a key factor for its compatibility with natural materials like plant roots. This can be exploited, for example, for extraterrestrial applications, where the harsh environment represents an obstacle for the development of organic plants growth and, in general terms, to sustain life in space.

ACKNOWLEDGMENTS

This project was supported by European Space Agency (ESA) AO/2–1749/20/NL/GLC "OSIP Off-Earth manufacturing and construction campaign-study scheme", part of the ESA's Discovery program.

DATA AVAILABILITY STATEMENT

Data available on request from the authors.

ORCID

E. A. Slejko https://orcid.org/0000-0003-4946-2612

REFERENCES

1. Rustemeyer P. History of CA and evolution of the markets. *Macromol Symp*. 2004;208:1-6.
2. Edgar KJ, Buchanan CM, Debenham JS, et al. Advances in cellulose ester performance and application. *Prog Polym Sci*. 2001; 26(9):1605-1688. https://linkinghub.elsevier.com/retrieve/pii/S0079670001000272
3. Park HM, Misra M, Drzal LT, Mohanty AK. "Green" nanocomposites from cellulose acetate bioplastic and clay: effect of eco-friendly triethyl citrate plasticizer. *Biomacromolecules*. 2004; 5(6):2281-2288.
4. Huang H, Dean D. 3-D printed porous cellulose acetate tissue scaffolds for additive manufacturing. *Addit Manuf*. 2020;31-(August):100927. doi:10.1016/j.addma.2019.100927
5. Zuo M, Pan N, Liu Q, Ren X, Liu Y, Huang TS. Three-dimensionally printed polylactic acid/cellulose acetate scaffolds with antimicrobial effect. *RSC Adv*. 2020;10(5):2952-2958.
6. Mohanty AK, Wibowo A, Misra M, Drzal LT. Development of renewable resource-based cellulose acetate bioplastic: effect of process engineering on the performance of cellulosic plastics. *Polym Eng Sci*. 2003;43(5):1151-1161.
7. Puls J, Wilson SA, Hölter D. Degradation of cellulose acetate-based materials: a review. *J Polym Environ*. 2011;19(1):152-165.
8. Makaya A, Pambaguian L, Ghidini T, Rohr T, Lafont U, Meurisse A. Towards out of earth manufacturing: overview of the ESA materials and processes activities on manufacturing in space. *CEAS Sp J*. 2023;15(1):69-75. doi:10.1007/s12567-022-00428-1
9. Sacco E, Moon SK. Additive manufacturing for space: status and promises. *Int J Adv Manuf Technol*. 2019;105(10):4123-4146.
10. Slejko EA, Sesto Gorella N, Makaya A, Gallina P, Scuor N, Seriani S. Vacuum 3D printing of highly filled polymeric matrix composites. *Acta Astronaut*. 2023;204(August):25-33. doi:10.1016/j.actaastro.2022.12.033
11. Schwarz D, Rouphael Y, Colla G, Venema JH. Grafting as a tool to improve tolerance of vegetables to abiotic stresses: thermal stress, water stress and organic pollutants. *Sci Hortic (Amsterdam)*. 2010;127(2):162-171.
12. Ropokis A, Ntatsi G, Kittas C, Katsoulas N, Savvas D. Effects of temperature and grafting on yield, nutrient uptake, and water use efficiency of a hydroponic sweet pepper crop. *Agronomy*. 2019;9(2):110. [cited 2023 May 8]. https://www.mdpi.com/2073-4395/9/2/110/htm
13. Kumar P, Rouphael Y, Cardarelli M, Colla G. Vegetable grafting as a tool to improve drought resistance and water use efficiency. *Front Plant Sci*. 2017;8:1130.
14. Colla G, Suãrez CMC, Cardarelli M, Rouphael Y. Improving nitrogen use efficiency in melon by grafting. *HortScience*. 2010; 45(4):559-565. [cited 2023 May 8]. https://journals.ashs.org/hortsci/view/journals/hortsci/45/4/article-p559.xml
15. Gaion LA, Braz LT, Carvalho RF. Grafting in vegetable crops: a great technique for agriculture. *Int J Veg Sci*. 2018;24(1):85-102. [cited 2023 May 8]. doi:10.1080/19315260.2017.1357062
16. Yang J, Wang H, Zhou B, Shen J, Zhang Z, Du A. Versatile direct writing of aerogel-based sol-gel inks. *Langmuir*. 2021; 37(6):2129-2139.
17. Chen C, Zhang R, Zhu J, et al. Direct writing polyvinylidene difluoride thin films by intercalation of nano-ZnO. *Polym Eng Sci*. 2021;61(6):1802-1809.
18. Dai L, Cheng T, Duan C, et al. 3D printing using plant-derived cellulose and its derivatives: a review. *Carbohydr Polym*. 2019; 203(March):71-86. doi:10.1016/j.carbpol.2018.09.027
19. Mohanty AK, Wibowo A, Misra M, Drzal LT. Effect of process engineering on the performance of natural fiber reinforced cellulose acetate biocomposites. *Compos Part A Appl Sci Manuf*. 2004;35(3):363-370.
20. Liu G, Bhat MP, Kim CS, Kim J, Lee KH. Improved 3D-printability of cellulose acetate to mimic water absorption in plant roots through Nanoporous networks. *Macromolecules*. 2022;55(5):1855-1865.
21. Paxton N, Smolan W, Böck T, Melchels F, Groll J, Jungst T. Proposal to assess printability of bioinks for extrusion-based bioprinting and evaluation of rheological properties governing bioprintability. *Biofabrication*. 2017;9(4):044107.
22. Mohammed AA, Algahtani MS, Ahmad MZ, Ahmad J. Optimization of semisolid extrusion (pressure-assisted microsyringe)-based 3D printing process for advanced drug delivery

application. *Ann 3D Print Med*. 2021;2:100008. doi:10.1016/j.stlm.2021.100008

23. Li N, Qiao D, Zhao S, Lin Q, Zhang B, Xie F. 3D printing to innovate biopolymer materials for demanding applications: a review. *Mater Today Chem*. 2021;20:20.
24. Zepnik S, Kabasci S, Kopitzky R, Radusch HJ, Wodke T. Extensional flow properties of externally plasticized cellulose acetate: influence of plasticizer content. *Polymers (Basel)*. 2013;5(3):873-889. [cited 2023 May 8]. https://www.mdpi.com/2073-4360/5/3/873/htm
25. Singer SJ, Mark H. On the structure of cellulose acetate molecules in acetone solution. *J Appl Phys*. 1948;19(1):97-101.
26. Pattinson SW, Hart AJ. Additive manufacturing of cellulosic materials with robust mechanics and antimicrobial functionality. *Adv Mater Technol*. 2017;2(4):1600084.
27. Gauss C, Pickering KL, Muthe LP. The use of cellulose in bio-derived formulations for 3D/4D printing: a review. *Compos Part C Open Access*. 2021;4(January):100113. doi:10.1016/j.jcomc.2021.100113
28. Fein K, Bousfield DW, Gramlich WM. Processing effects on structure, strength, and barrier properties of refiner-produced cellulose nanofibril layers. *ACS Appl Polym Mater*. 2021;3(7):3666-3678.
29. Gasoto SC, Schneider B, Setti JAP. Study of the pulse of peristaltic pumps for use in 3D extrusion bioprinting. *ACS Omega*. 2022;7(28):24091-24101. doi:10.1021/acsomega.1c07093
30. Klespitz J, Kovács L. Peristaltic pumps—a review on working and control possibilities. SAMI 2014—IEEE 12th International Symposium on Applied Machine Intelligence and Informatics, Proceedings. 191–194. 2014.
31. McIntyre MP, van Schoor G, Uren KR, Kloppers CP. Modelling the pulsatile flow rate and pressure response of a roller-type peristaltic pump. *Sens Actuator A Phys*. 2021;325:112708. https://linkinghub.elsevier.com/retrieve/pii/S0924424721001710
32. Biviano MD, Paludan MV, Christensen AH, Østergaard EV, Jensen KH. Smoothing oscillatory peristaltic pump flow with bioinspired passive components. *Phys Rev Appl*. 2022;18(6):1. doi:10.1103/PhysRevApplied.18.064013
33. Ding Y, Ying S. Cell structure, density and impact strength of cellulose acetate foamed with supercritical carbon dioxide. *Cell Polym*. 2015;34(6):339-352.
34. Ferrarezi MMF, Rodrigues GV, Felisberti MI, Gonçalves MDC. Investigation of cellulose acetate viscoelastic properties in different solvents and microstructure. *Eur Polym J*. 2013;49(9):2730-2737.
35. Max JJ, Chapados C. Infrared spectroscopy of acetone-water liquid mixtures. Ii. *Mol Model J Chem Phys*. 2004;120(14):6625-6641.
36. Zugenmaier P. Characterization and physical properties of cellulose acetates. *Macromol Symp*. 2004;208:81-166.
37. de Beukelaer H, Hilhorst M, Workala Y, Maaskant E, Post W. Overview of the mechanical, thermal and barrier properties of biobased and/or biodegradable thermoplastic materials. *Polym Test*. 2022;116(October):107803. doi:10.1016/j.polymertesting.2022.107803
38. Okuzono T, Ozawa K, Doi M. Simple model of skin formation caused by solvent evaporation in polymer solutions. *Phys Rev Lett*. 2006;97(13):1-4.
39. Punati VS, Tirumkudulu MS. Modeling the drying of polymer coatings. *Soft Matter*. 2022;18(1):214-227.
40. Akhoundi B, Behravesh AH. Effect of filling pattern on the tensile and flexural mechanical properties of FDM 3D printed products. *Exp Mech*. 2019;59(6):883-897.
41. Pazhamannil RV, Jishnu Namboodiri VN, Govindan P, Edacherian A. Property enhancement approaches of fused filament fabrication technology: a review. *Polym Eng Sci*. 2022;62(5):1356-1376.
42. Xu C, Cheng K, Liu Y, et al. Effect of processing parameters on flexural properties of 3D-printed polyetherketoneketone using fused deposition modeling. *Polym Eng Sci*. 2021;61(2):465-476.
43. Ambone T, Torris A, Shanmuganathan K. Enhancing the mechanical properties of 3D printed polylactic acid using nanocellulose. *Polym Eng Sci*. 2020;60(8):1842-1855.
44. Alturkestany MT, Panchal V, Thompson MR. Improved part strength for the fused deposition 3D printing technique by chemical modification of polylactic acid. *Polym Eng Sci*. 2019;59(s2):E59-E64.
45. Crank J. *The Mathematics of Diffusion*. 2nd ed. Oxford University Press; 1975.
46. Crank J. A theoretical investigation of the influence of molecular relaxation and internal stress on diffusion in polymers. *J Polym Sci*. 1953;11(2):151-168. doi:10.1002/pol.1953.120110206
47. De Wilde WP, Shopov PJ. A simple model for moisture sorption in epoxies with sigmoidal and two-stage sorption effects. *Compos Struct*. 1994;27(3):243-252. https://linkinghub.elsevier.com/retrieve/pii/026382239490085X
48. Mensitieri G, Scherillo G. Environmental resistance of high performance polymeric matrices and composites. *Wiley Encyclopedia of Composites*. John Wiley & Sons, Inc.; 2012. doi:10.1002/9781118097298.weoc074
49. Ritger PL, Peppas NA. A simple equation for description of solute release I. Fickian and non-fickian release from non-swellable devices in the form of slabs, spheres, cylinders or discs. *J Control Release*. 1987;5(1):23-36. https://linkinghub.elsevier.com/retrieve/pii/0168365987900344
50. Ritger PL, Peppas NA. A simple equation for description of solute release II. Fickian and anomalous release from swellable devices. *J Control Release*. 1987;5(1):37-42. https://linkinghub.elsevier.com/retrieve/pii/0168365987900356
51. Witono JR, Noordergraaf IW, Heeres HJ, Janssen LPBM. Water absorption, retention and the swelling characteristics of cassava starch grafted with polyacrylic acid. *Carbohydr Polym*. 2014;103(1):325-332. doi:10.1016/j.carbpol.2013.12.056
52. Khoshtinat S, Carvelli V, Marano C. Moisture absorption measurement and modelling of a cellulose acetate. *Cellulose*. 2021;28(14):9039-9050. doi:10.1007/s10570-021-04114-z
53. Mathew AP, Gong G, Bjorngrim N, Wixe D, Oksman K. Moisture absorption behavior and its impact on the mechanical properties of cellulose whiskers-based polyvinylacetate nanocomposites. *Polym Eng Sci*. 2011;51(11):2136-2142. doi:10.1002/pen.22063

How to cite this article: Slejko EA, Sesto Gorella N, Gasparini R, Scuor N, Seriani S. Tailoring 3D printed cellulose acetate properties produced via direct ink writing: Densification through over-extrusion and evaporation rate control. *Polym Eng Sci*. 2023;63(11):3786-3797. doi:10.1002/pen.26484